Photoacoustics 4 (2016) 91–101

Contents lists available at ScienceDirect

Photoacoustics

journal homepage: www.elsevier.com/locate/pacs

All-optical optoacoustic microscopy based on probe beam deflection technique

Saher M. Maswadi[a,b,h,*], Bennett L. Ibey[c], Caleb C. Roth[d], Dmitri A. Tsyboulski[e], Hope T. Beier[f], Randolph D. Glickman[g,h], Alexander A. Oraevsky[e]

[a] Oak Ridge Institute for Science and Education, 4141 Petroleum Road, JBSA Fort Sam Houston, TX 78234, USA
[b] Department of Physics and Astronomy, University of Texas at San Antonio, One UTSA Circle, San Antonio, TX 78249, USA
[c] Radio Frequency Bioeffects Branch, Bioeffects Division, Human Effectiveness Directorate, 711th Human Performance Wing, Air Force Research Laboratory, 4141 Petroleum Road, JBSA Fort Sam Houston, TX 78234, USA
[d] School of Medicine, Dept. of Radiological Sciences, University of Texas Health Science Center San Antonio, 7703 Floyd Curl Drive, San Antonio, TX 78229, USA
[e] TomoWave Laboratories, 6550 Mapleridge St., Houston, TX 77081, USA
[f] Optical Radiation Branch, Bioeffects Division, Human Effectiveness Directorate, 711th Human Performance Wing, Air Force Research Laboratory, 4141 Petroleum Road, JBSA Fort Sam Houston, TX 78234, USA
[g] School of Medicine, Dept. of Ophthalmology, University of Texas Health Science Center San Antonio, 7703 Floyd Curl Drive, San Antonio, TX 78229, USA
[h] EchoLase, Inc., 5234 Tomas Circle, San Antonio, TX 78240, USA

ARTICLE INFO

Article history:
Received 10 November 2015
Received in revised form 2 February 2016
Accepted 20 February 2016
Available online 24 February 2016

Keywords:
Optical resolution photoacoustic imaging
Optoacoustic tomography
Probe beam deflection technique
All optical optoacoustic system
Non-contact acoustic sensor
Backward mode optoacoustic microscopy

ABSTRACT

Optoacoustic (OA) microscopy using an all-optical system based on the probe beam deflection technique (PBDT) for detection of laser-induced acoustic signals was investigated as an alternative to conventional piezoelectric transducers. PBDT provides a number of advantages for OA microscopy including (i) efficient coupling of laser excitation energy to the samples being imaged through the probing laser beam, (ii) undistorted coupling of acoustic waves to the detector without the need for separation of the optical and acoustic paths, (iii) high sensitivity and (iv) ultrawide bandwidth. Because of the unimpeded optical path in PBDT, diffraction-limited lateral resolution can be readily achieved. The sensitivity of the current PBDT sensor of 22 μV/Pa and its noise equivalent pressure (NEP) of 11.4 Pa are comparable with these parameters of the optical micro-ring resonator and commercial piezoelectric ultrasonic transducers. Benefits of the present prototype OA microscope were demonstrated by successfully resolving micron-size details in histological sections of cardiac muscle.

1. Introduction

New discoveries in functional and molecular optoacoustic microscopy enabled by imaging of changes in metabolism, blood flow and hemodynamics, blood oxygenation, chemical composition of tissue and absorption spectrum changes associated with genetic processes, proved to be indispensable for the advancement of biomedical science [1–6]. Although most high-resolution, pure-optical microscopy methods are capable of detecting endogenous optical contrast such as optical scattering, fluorescence or bioluminescence, these methods do not directly detect the optical absorption of tissue chromophores. Consequently, the need for high-resolution functional and molecular imaging based on the optical absorption and at significantly greater depth in biological tissues has been recognized recently, and as a result, optical-resolution optoacoustic (photoacoustic) microscopy has emerged [4,7–11]. Functional and molecular imaging, using optoacoustic technologies, has gained great interest among the biological community as a method to detect, monitor and quantify activity or the interactions of specific properties in living tissues, organs or even individual cells. Optoacoustic microscopy (OAM) is based on imaging optically absorbing microstructures in the sample by recording transient pressure waves generated by instantaneous (pulsed) laser heating as a result of thermal energy deposition by the absorbed light and launched by thermal expansion of the heated medium. In the typical biomedical application of OAM, a focused pulsed-laser beam is directed onto the biological tissue to generate ultrasound waves. An image of the absorbed optical energy is acquired by raster-scanning the focal point across the imaging area or a volume. The OA image has the same resolution,

* Corresponding author at: EchoLase, Inc., 5234 Tomas Circle, San Antonio, TX 78240, USA.
E-mail address: maswadi@echolase.com (S.M. Maswadi).

http://dx.doi.org/10.1016/j.pacs.2016.02.001

but a significantly higher contrast, compared to bright field optical microscopy [12].

The majority of OAM systems introduced to date, with a few exceptions [13–18], use a piezoelectric-based method of ultrasound detection [7,10,11,19]. Two types of OAM configurations can be distinguished as backward and forward modes, based on the positioning of the excitation and detection systems relative to the sample. In the forward mode, the excitation optics and the detection element are positioned on different sides of the sample, and the optoacoustic signal propagates forward along the optical beam. Forward mode places no restrictions on the optical elements used for excitation beam focusing, but instead limits the types of samples that can be used for imaging. Only relatively thin samples that are optically and acoustically transparent can be used in this mode [8]. Conversely, with the backward mode, where excitation and detection elements are on the same side relative to the sample, and the optoacoustic signal propagates backward relative to the optical excitation beam, there is no restriction on sample type, making this mode generally applicable in vivo and used by most researchers in live animals. However, with the backward mode configuration, the optical and acoustic paths must be separated, which is accomplished by using optical elements, including prisms [7,9], parabolic reflectors [11], etc., or piezoelectric elements of special shape, such as needle [20] or ring-shaped transducers [21]. Using additional elements to separate the optical path from the acoustic path introduces undesirable wave-front distortions in both paths and negatively impacts the image quality, ultimately limiting the capability of this technique [7,9,11,21]. While it is difficult to achieve sub-micron resolution in the backward mode OA microscopy based on piezoelectric transducers because of wave-front distortions that occur in the components placed between the tissue and the objective lens to separate the acoustic wave from the laser excitation beam, such high-resolution is readily achieved in the system described below. Piezoelectric sensing was also reported without optical-acoustic separation to achieve subwavelength resolution when using a miniature or needle transducer placed just below an objective lens [20]; however, the use of additional elements, including different shapes of piezoelectric elements or even custom types of objective lenses, generally limits the minimum working distance in relation to the sample or interacts with the excitation beam by partially blocking or deforming the beam profile. These perturbations reduce the numerical aperture (NA) of the excitation beam focusing optics and as a result diminish the optical quality. Consequently, most of the optical resolution photoacoustic microscopy setups introduced up to this date have failed to achieve diffraction-limited resolution [7,9–11,21].

Several research groups have utilized optical techniques to detect generated optoacoustic pressure waves to overcome some of the limitations in optoacoustic tomography and microscopy. As a result, optical methods of ultrasound detection are recognized in the optoacoustic imaging community and have been able to achieve levels of sensitivity approaching those of the piezoelectric transducers [13–15,22]. Nonetheless, the number of reports describing all-optical optoacoustic imaging techniques remains rather limited. The most notable examples of all-optical optoacoustic imaging techniques are Fabry–Perot interferometry and micro-ring resonator sensors, each with reported sensitivity levels of 6.8 Pa [18], 29 Pa [15], or 210 Pa [23], respectively. Micro-ring resonator OAM imaging setups were demonstrated in forward [15] and backward [18] mode imaging applications with optical resolution. In OAM, OA signals are generated from micro- or submicron objects, e.g. cells or small capillaries. These OA signals usually contain high frequency components that become highly attenuated even after passing less than 1 mm distance from the source, resulting in signals weaker than those generated in OA tomography. Therefore, sensitivity of an OA microscopy system is perhaps the most important property that defines its utility and the scope of its use. An inherent flaw with most OAM systems that reduces system sensitivity is the limited dynamic range of piezoelectric detectors with respect to conversion of pressure into voltage. To expand the scope and the range of applications of OAM technique, novel analytical instrumentation with better resolution and sensitivity is needed. Although constantly improving, axial and lateral resolution limits of previously introduced optoacoustic microscopes have not achieved the resolution levels of optical microscopy techniques [7,9–11,21]. To ensure further progress in the field of optoacoustic

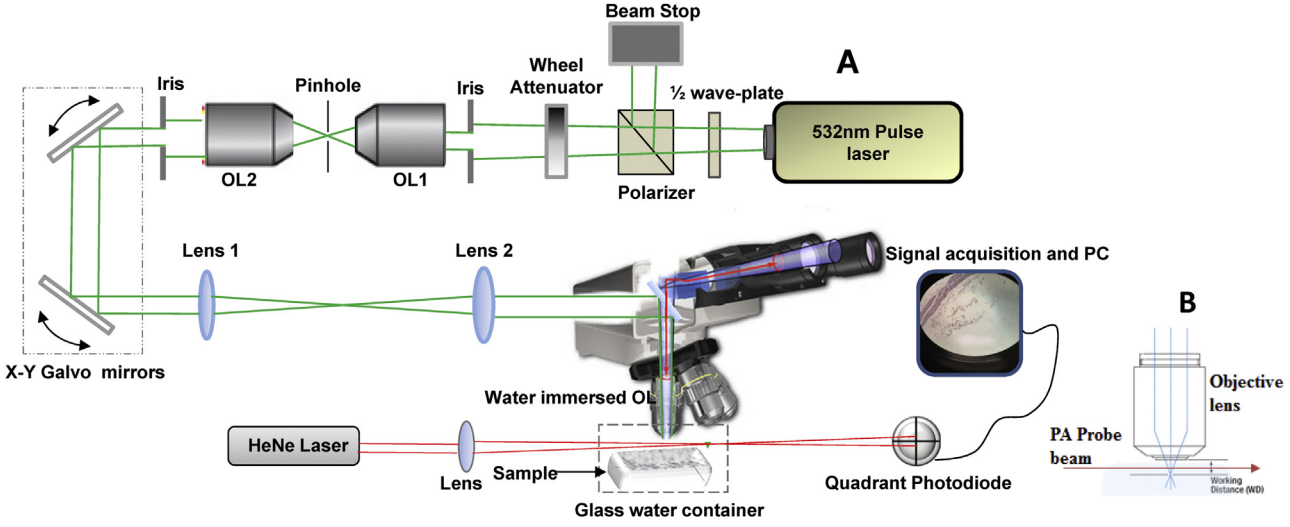

Fig. 1. (A) Schematic diagram of all-optical OAM system based on PBDT integrated into an optical microscope (Zeiss) to allow for simultaneous acquisition of optoacoustic and optical imaging. The OA scanning was accomplished using galvanometer-mounted mirrors. OL: Objective lens. (B) A diagram to show the propagation of the probe sensor within the working distance of the microscope objective lens to detect pressure waves generated in the sample.

imaging, novel ultrasound detection technologies must be developed.

In this paper, we introduce a novel OAM design that utilizes an all-optical method, the probe beam deflection technique (PBDT), for ultrasound generation and detection [17,24–27]. A recent review of all-optical OAM methods [28] did not mention the PBDT, which emphasizes the novelty of this method in optoacoustic microscopy. The acoustic waves generated in the sample propagate towards the CW probe laser beam and cause transient changes of refractive index in the coupling medium, which result in the probe beam deflection. A balanced 2D array of photodiodes detects the probe beam deflection as a differential signal with magnitude proportional to the amplitude of the acoustic pressure wave. Because of the unimpeded optical path in PBDT, high numerical aperture objective lenses (NA ~1) were employed in this microscope to achieve diffraction-limited lateral resolution of <0.5 μm at 532 nm while optically scanning the excitation beam using galvanometer-mounted mirrors. With this design, we demonstrate the capability of high-resolution, all-optical optoacoustic microscopy with a non-contact method (ultrasound coupling through water with no detector in physical contact with the water) that uses no elements between the objective lens and samples. This arrangement provides the system designer maximum flexibility in the selection of objective lenses, i.e. low NA lenses for larger field areas and high NA lenses for maximum resolution, as well as demonstrating the OAM potential for addressing an important set of problems and biomedical applications. The all-optical optoacoustic microscopy system offers a number of benefits in terms of achievable lateral and axial resolution, sensitivity, robustness, and versatility.

2. Materials and methods

2.1. Microscope setup

Fig. 1 shows the implementation of a basic, non-contact all-optical OA microscope built on a commercial optical microscope (Zeiss Axio Scope.A1, Carl Zeiss Microscopy, Jena, Germany) modified for laser scanning. Optoacoustic excitation was performed by Nd:YAG Q-switch pulse laser (Big Sky Laser Technologies, now Quantel, Bozeman, MT) at 532 nm wavelength with 6 ns pulse duration and a 20 Hz pulse repetition frequency. Excitation light was delivered to the microscope objective through a series of optical components including a half-wave plate-polarizer combination for light attenuation followed by a continuously variable optical density filter wheel to fine-tune the intensity. The beam was spatially filtered by passing through a 15 μm pinhole using a 20× objective lens and then collimated by another objective lens as shown in Fig. 1. Image scanning was performed optically by changing the optical path of the excitation laser beam using a dual axis X–Y galvanometer-mounted mirror system (GVS002, Thorlabs, Newton, NJ) before passing through the microscope. The standard illumination optics of the microscope were removed and replaced with a telescope assembly (L1, L2) consisting of a 50 mm achromatic scan lens and a 165 mm Zeiss tube lens to overfill the back focal plane of the objective to ensure a diffraction-limited

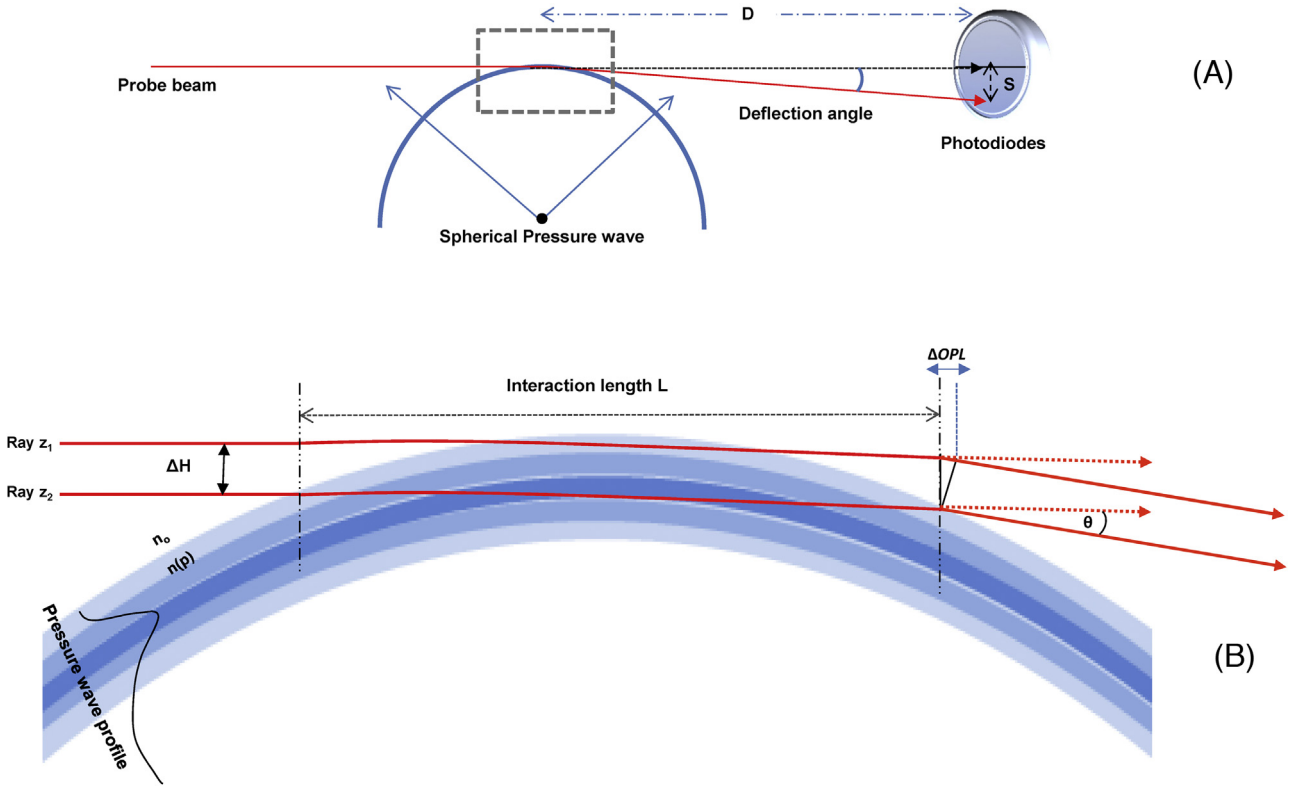

Fig. 2. Overview of PBDT. (A) Schematic illustration of probe beam deflection resulting from interaction with a spherical pressure wave, as in the case of OA microscopy. The probe beam, after interacting with the pressure wave, impinges on a photodiode position detector. The variable D represents the distance of the photodiodes from the interaction regions, and the variable S denotes the displacement of the beam along the face of the photodiodes. These variables are used in Eqs. (2) and (3), in the text, to derive the amplitude of the differential signal from the position detector. (B) The interaction length of the probe beam and the pressure wave is limited to a small distance at the point where the probe beam intersects the pressure wave front. The deflection of the beam occurs throughout the interaction length as a function of the integrated gradient of refractive index changes in the medium; in this figure, for illustrative purposes, the beam deflection is portrayed as occurring at a single point at the end of the interaction length, L. Δ*H* is the probe beam diameter, ΔOPL is the difference in the optical path length between two rays, $z_1$and z_2, in the deflected beam, θ is the beam deflection angle, and n(p) designates the refractive index as a function of pressure.

spot. The telescope primarily served to expand the laser beam to ensure it completely filled the back aperture of the objective lens; the lens elements OL1 and OL2 were matched, and the beam leaving OL2 was only 2–3 mm in diameter. This small diameter was necessary because the galvanometer-mounted mirrors only allowed for a beam diameter <5 mm. The telescope then expanded the beam to fill the back focal plane diameter of the objective. The position of the lenses and collimation of the laser beam was verified with a shearing interferometer. A dichroic mirror allowed simultaneous optical imaging during the optoacoustic scanning while delivering part of the excitation light into the water immersion objective lens with NA = 1.0 and working distance of 2.5 mm (Zeiss Objective W Plan-Apochromat 40x/1.0 DIC).

2.2. Probe beam deflection technique

The probe beam deflection technique PBDT, as a non-contact method, was used to detect generated pressure waves passing through a probe beam as shown in Fig. 1B. The propagation of the pressure wave produces a local density gradient, which alters the refractive index of the coupling medium (in this case DI water) which is directly proportional to pressure (piezo-optic coefficient $dn/dP = 1.35 \times 10^{-5}$ bar^{-1} for water [29]), leading to beam deflection. PBDT has been extensively described in our previous work [17,24–27]. In short, the sensor beam interacts with a spherical shape pressure wave generated from a point source and the interaction length between the probe beam and the pressure waterfront is limited to a small area or just a point of interaction as illustrated in Fig. 2. Deflection of the probe beam is a function of the change of refractive index with pressure (dn/dP) at the interaction area. A 21 mW continuous wave (CW) Helium–Neon (HeNe) laser (Model HNL210L, Thorlabs, Newton, NJ) with 0.7 mm beam diameter was used as a sensor beam for the PBDT and focused to ~90 μm beam waist diameter just below the microscope objective lens and 2 mm above the sample using a 10 cm focal length lens. Beam position was monitored with a quadrant photodiode SPOT-9DMI (OSI Optoelectronics, Hawthorne, CA) coupled to a custom differential amplifier with 20 dB gain and 0–25 MHz bandwidth. The deflection signals were digitized using a Tektronix e*Scope (TDS 3054B, Tektronix, Beaverton, OR) at 500 MHz with a 50 ohm terminator and then captured using a custom LabVIEW program (National Instruments, Austin, TX). The LabVIEW program also controlled laser triggering and galvanometer mirror scanning using digital and timing boards (National Instruments NI USB-6251). The amplitude of the beam deflection was directly proportional to the magnitude of the refractive index gradient, which enabled the reconstruction of an image of the sample, based on the spatial distribution of optical absorbers within the sample.

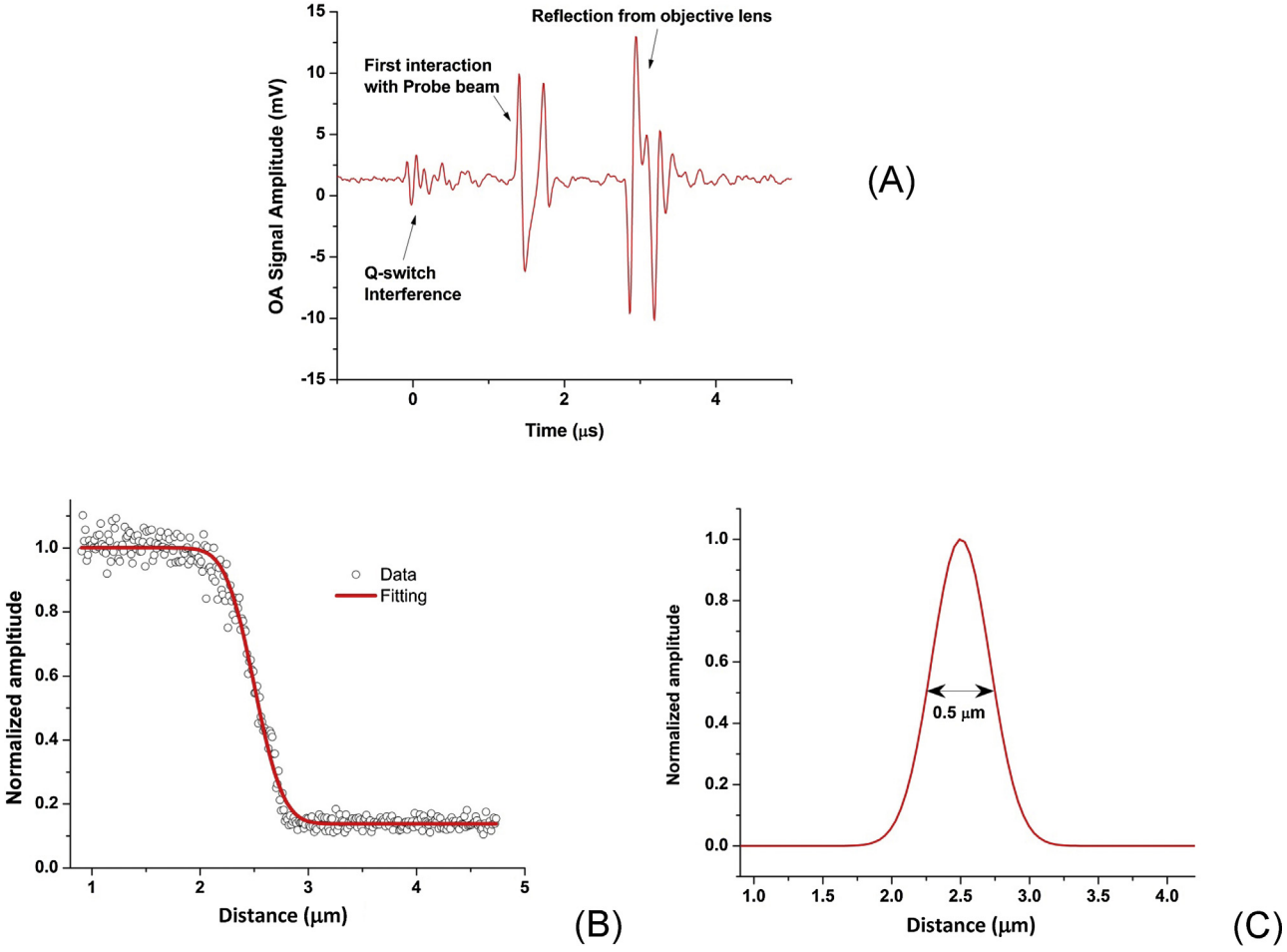

Fig. 3. (A) OA signal recorded using PBDT during scanning showing the passive sensing capability. (B) Lateral resolution measurement of the OA system using edge spread function ESF. (C) Point spread function derived from the fitted ESF; the measured resolution was 0.5 μm FWHM.

2.3. Biological samples

Biological samples were also used to demonstrate the imaging capability of PBDT. Tissue samples were donated and not specifically procured for this research at the Air Force Research Laboratories. The donated tissues consisted of 5 μm thick sections of cardiac muscle harvested from a male rhesus macaque (*Macaca mulatta*), and stained with hematoxylin and eosin using standard histological protocols. A single blood cell was also imaged from one of the sections of the cardiac tissue. Tissues sections were not covered with a glass coverslip to prevent attenuation of acoustic waves from these samples.

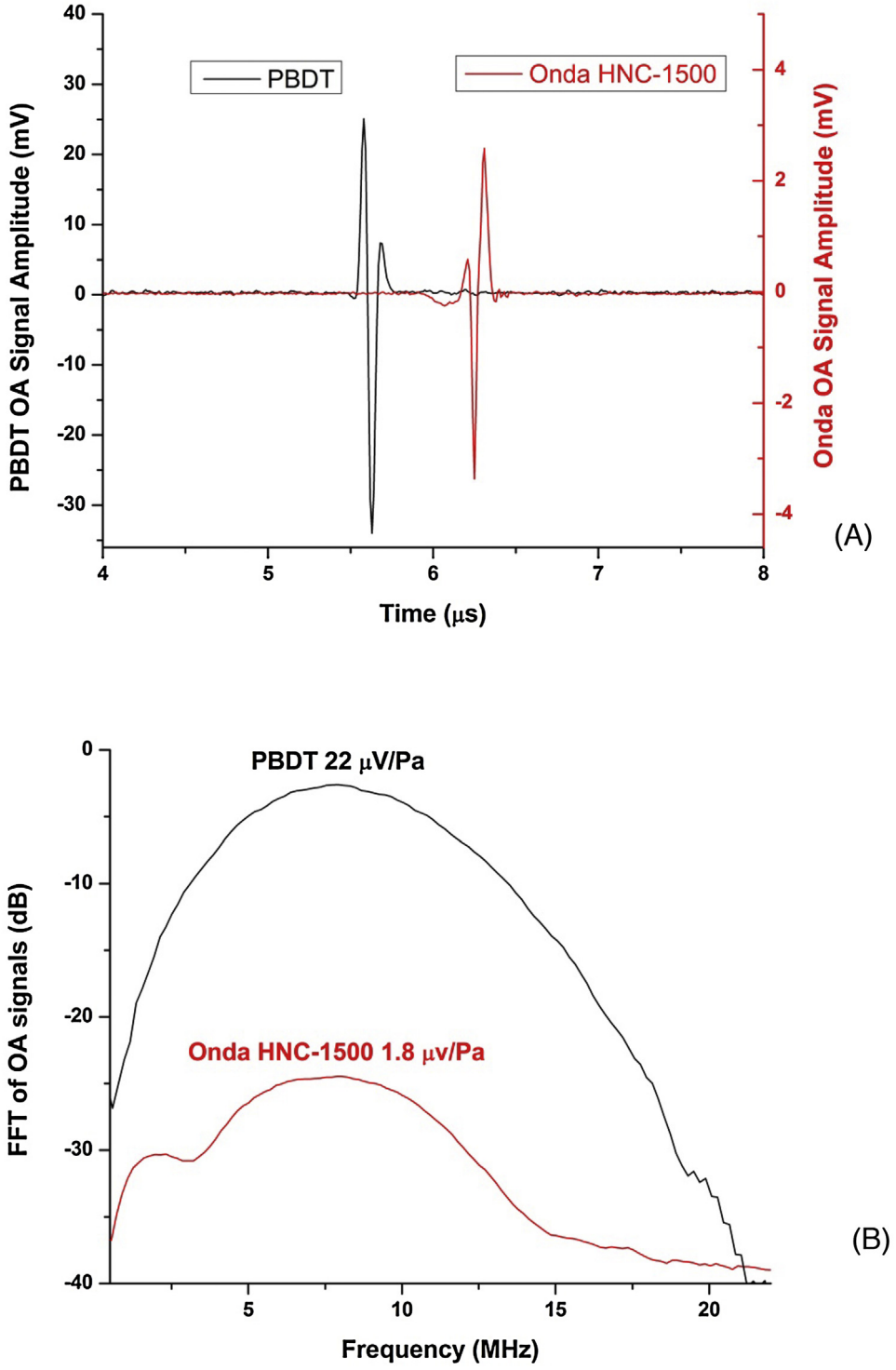

Fig. 4. (A) OA signals simultaneously recorded using piezoelectric hydrophone and PBDT from a point source. The left Y-scale is for the PBDT signal while the right Y-scale is for the signal recorded by HNC-1500 hydrophone. (B) FFT of the recorded OA signals showing the measured relative sensitivity levels of both methods.

3. Results and discussion

3.1. System resolution

Lateral imaging resolution was measured by scanning across a sharp edge of an Air Force resolution target (USAF-1951) located at the focal point of the objective lens with step size of 12 nm. Fig. 3A shows a typical OA signal generated from an absorbing region of the resolution target, which demonstrates the passive or non-contact sensing capability. First, the pressure wave interacts with the probe beam then reflects back from the surface of the objective lens to interact again with the probe sensor as shown in Fig. 3A. Imaging resolution was measured by using an edge spread function (ESF) technique. The data were fitted by the least square function of the system, then the point spread function was obtained by computing the first derivative of the fit as shown in Fig. 3A and B [30]. The Full Width at Half Maximum (FWHM) of the Gaussian PSF was measured to be <0.5 μm as shown in Fig. 3B. For a given NA of 1, and the imaging wavelength of 532 nm, the diffraction-limited resolution was calculated as $0.5\lambda/NA$, equal to 0.27 μm. The experimentally measured resolution is less than the theoretically calculated resolution due to the imperfect correction of refractive errors through the series of optical components. This resolution was likely reduced by the aberrations present in a telescopic 4F system, which may potentially be eliminated with better quality optical components [31]. Importantly, for the PBDT detection method described here, the acoustic sensor did not limit the optical resolution, unlike piezoelectric or other opaque detectors, which must be inserted into the optical beam path.

Typically, the axial resolution is determined by the spatial width of the detected optoacoustic signal, which is determined in the case of PBDT by the diameter of the probe beam at the point of interaction with the pressure wave-front. In this setup the probe beam diameter at the interaction area was approximately 90 μm, which offered a theoretical detection bandwidth of 17 MHz (equal to the speed of sound/beam diameter) and the corresponding acoustic resolution at the full width half maximum (FWHM) was about 60 μm. However, in the case of optical resolution OAM, where depth of field (DOF) is much smaller and can be estimated ($DOF \approx \lambda \frac{n}{NA^2} = 0.7\mu m$), Z-axial resolution is primarily defined by the depth of field of the imaging system where objects out of focus absorb significantly less light and generate less signal. We confirmed experimentally that that the depth of field and the depth resolution was about 1 μm, but the lack of precision scanning along the depth-axis in this current setup did not permit a more accurate measurement.

3.2. System sensitivity measurements

To determine the sensitivity of the PBDT in this experimental configuration, OA signals generated from the same source were simultaneously measured by PBDT and a calibrated HNC-1500 hydrophone (Onda, Sunnyvale, CA) with a sensitivity of 1.8 μV/Pa (−234 dB relative to 1 V/μPa at 10 MHz). Laser pulses focused with a 5× objective lens (NA = 0.13) on a thin absorbing layer were used to create spherical acoustic waves. Both the hydrophone and the probe beam were positioned at 5 mm distance from the source at the same time, and the transient pressure profiles were recorded

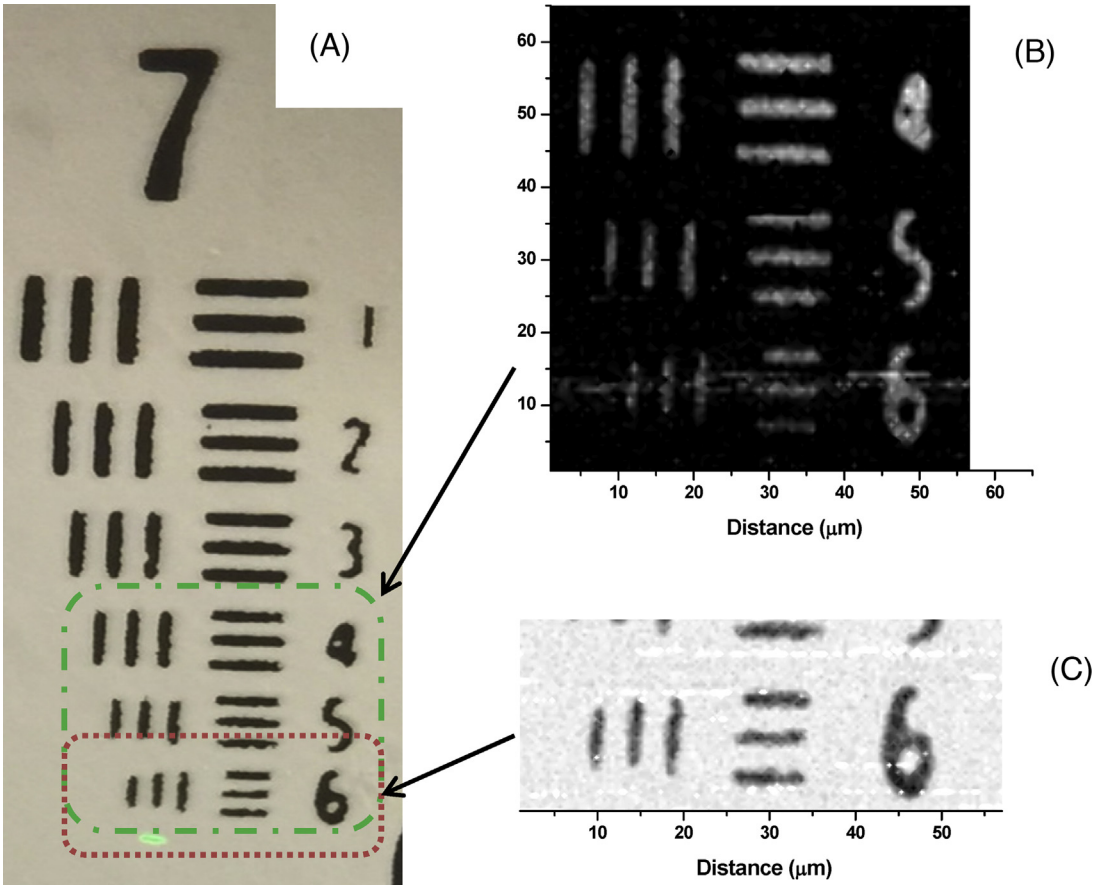

Fig. 5. (A) Optical image of US Air Force resolution target group 7 showing the region that was scanned for the OA inage. (B) OA image showing part of group 7 scanned with step resolution of 0.7 μm. (C) Higher resolution OA image of smallest region of the target (region 6 in group 7), scanned with step resolution of 0.47 μm. The pixel value is inverted compared to the image in panel B.

using both devices. Recorded signals from both sensors were averaged at the same time as shown in Fig. 4A where the left Y-scale corresponds to PBDT and the right Y-scale to the HNC-1500 hydrophone. Fast Fourier Transform (FFT) spectra were obtained from the recorded signal (Fig. 4B) and showed that PBDT detector possesses approximately 21.5 dB higher sensitivity (22 μV/Pa) compared to the Onda hydrophone. This sensitivity level is higher than the sensitivity of many commercial piezoelectric transducers (e.g. ~3 μV/Pa at the peak, 40 MHz central frequency, 50 MHz bandwidth) [32]. An advantage of using PBDT is the ability to position the probe beam in close proximity to the pressure source, thus allowing one to achieve significantly higher dynamic range of detected optoacoustic signals.

Noise equivalent pressure (NEP) was obtained by measuring the noise level of both Onda hydrophone and PBDT detectors at the output of their corresponding amplifiers, each with gain of 20 dB, and calculating NEP [Pa] as (Noise [μV]/Amp Gain)/Sensitivity [mV/Pa]) as described in [32,33]. The signal from the Onda HNC-1500 hydrophone was amplified by 20 dB with a matched amplifier (AH-2010, Onda) resulting in the noise level of 0.33 mV on the output measured as a standard deviation from zero level. Consequently, NEP = 18.3 Pa was determined for the Onda system. Our measurement of NEP in the optoacoustic detector based on Onda HNC-1500 hydrophone agrees well with a previously reported measurement of 19 Pa[15]. The measured noise level for PBDT was 2.5 mV after the 20 dB differential amplifier, which results in approximately 11.4 Pa NEP for the current PBDT configuration. It was noted that the recorded noise level was negligibly different with and without light incident on the photodiodes. Thus, the current sensitivity level of PBDT is at least comparable if not greater than most piezoelectric detectors with larger active sensors.

3.3. Optoacoustic microscopic imaging

To evaluate the OAM imaging capability, different samples were used. These samples included a US Air Force resolution test target, as well as fixed biological samples. Fig. 5 shows OA images of the

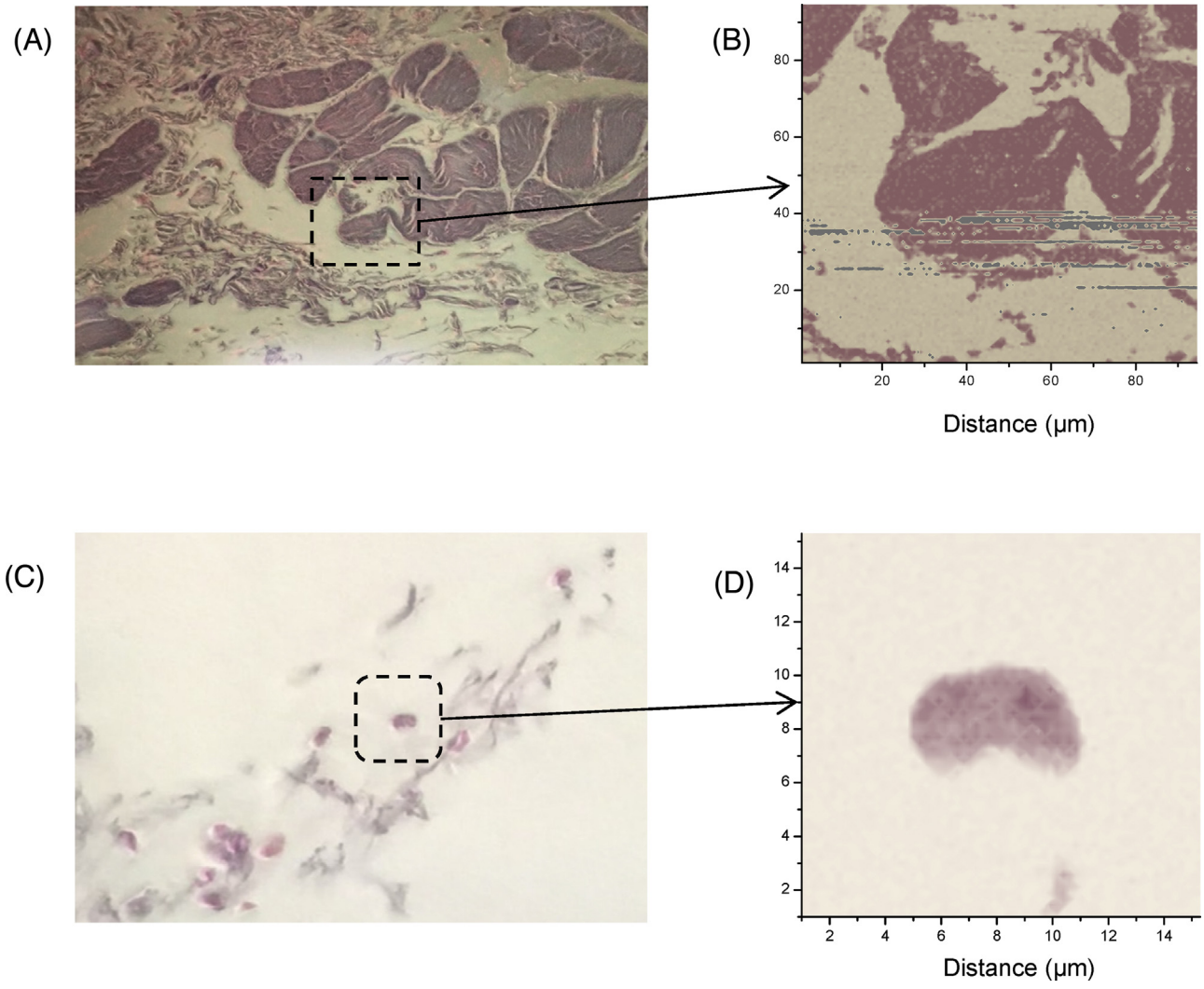

Fig. 6. (A) Optical image of a 5 μm section of cardiac tissue mounted on a glass slide. The dotted outline indicates the region of the sample that was scanned for the OA image. (B) OA image of the scanned area of the cardio tissue with 134 × 134 steps and step resolution of 0.7 μm. (C) Optical image (left) of a sample with tissue debris and cluster of lysed red blood cells. The box indicates the area that was scanned for OA image acquisition. (D) OA image of the single erythrocyte, scanned with 65 × 65 steps and step size of 0.23 μm. The color palettes assigned to the OA pixel values were adjusted to match the colors of the optical images.

resolution target scanned at different step sizes (i.e. resolutions). Notably, image acquisition was a slow process with the current system because of the low repetition rate of the pulse laser (20 Hz) and the slow data acquisition rate from the digital scope. Signals were averaged 4 or 8 times at every step (≤1 s was required to acquire the data and reset the scope). No signal processing or filtration was used; the peak-to-peak signals were recorded as a function of time and then plotted using Origin® software (OriginLab®, Northampton, MA). Fig. 5A shows the optical image of group 7 in the resolution target which was captured after the OA scans, while Fig. 5B shows a scanned optoacoustic image of part of group 7 with step resolution of 0.7 μm. The slow scanning process precluded scanning the entire group. Fig. 5B demonstrates the higher resolution capability of OA imaging with step size of 0.47 μm scanning region 6 of group 7, which is the smallest size in the target. The pixel color values of Fig. 5B are inverted in Fig. 5C to display a white background, so that the OA image resembles the optical image shown in Fig. 5A. These OA images are an excellent demonstration of high resolution OA scanning while capturing a standard optical image at the same time.

Optical and optoacoustic images of histological sections of the cardiac tissue were captured as shown in Fig. 6 to demonstrate the resolution and sensitivity of our OAM system. The energy of the pulsed laser was measured to be less than 50 nJ per pulse with 4 averages per step, and no damage to the tissue sample resulted during the complete OA scan. Fig. 6A is the optical image of the tissue section, while Fig. 6B shows an OA image of a scanned area of 93.8 × 93.8 μm with 0.7 μm step resolution and 17,956 steps. In this scanning-beam system, the size of the scan area was determined by the field of view of the objective lens; using a lower NA objective lens would have provided a larger field of view, but at a lower resolution. To increase the effective scan area, a mechanical translation stage could be used to move the sample in addition to, or instead of, the optical scanning, while maintaining the resolution. The gray pixels in the image shown in Fig. 6B are bad pixels resulting from misalignment of the probe beam at the photodiode during the long scanning time (hours) caused by room vibrations or mechanical drift of the microscope optics. In another region of the sample slide (the optical image of this region is shown in Fig. 6C), a single erythrocyte was identified and scanned at a higher resolution of 0.23 μm step size. The size of the cell is about 6 μm along its long axis (Fig. 6D). The optoacoustic image in Fig. 6D shows some of the details of the red blood cell with good resolution and sensitivity. Again the slow scanning process at the current system prevented us from scanning a larger area with high resolution.

3.4. PBDT sensitivity parameters

To evaluate sensitivity of the PBDT detector, namely *V(P)*, where *V* is the readout voltage change in response to the change in pressure d*P*, first we consider a beam with a width of ΔH passing through a medium with a refractive index gradient as a function of pressure as shown in Fig. 2. The pressure induced changes in the refractive index distribution n that can approximated as $n(P) = n_m + \alpha P$, where α is the piezo-optic coefficient dn/dP of the medium (e.g. α for water is 1.35×10^{-5} bar^{-1}) and n_m is the refractive index of the medium (e.g. water in this case). For a simple model, i.e. when the change of the refractive index dn across the beam ΔH is small, the beam deflection angle θ is given as $\theta \approx \frac{\Delta OPL}{\Delta H}$, where ΔOPL is the difference of the optical path lengths $(OPL = \int_0^L n(P)dl)$ of two rays separated by ΔH propagating along path l through a pressure wavefront with interaction length of L; thus θ can be expressed as:

$$\theta \approx \frac{L}{n_m \Delta H}\frac{dn}{dP}\alpha P \tag{1}$$

The deflection angle is inversely proportional to the refractive index of the coupling medium, n_m (e.g., the water contained between the lens and the sample), and it should be noted that the refractive index of water will be replaced by that of air as soon as the beam exits the water container and travels to the photodiode sensor. Ideally, the probe beam should be small and collimated along the interaction length to achieve the best sensitivity and resolution.

For the detector positioned at distance D from the point of interaction, the displacement of the beam S from the center of the detector equals $D\theta$. Assuming direct proportionality between the incident power density and the generated current at each segment of the photodiode, the differential signal output V can be written as:

$$V = GI_0\frac{1}{\sigma\sqrt{2\pi}}\left[\int_{-\infty}^{S} e^{-\frac{(x-S)^2}{2\sigma^2}}dx - \int_{S}^{+\infty} e^{-\frac{(x-S)^2}{2\sigma^2}}dx\right] \tag{2}$$

where G is the power to voltage conversion efficiency, which depends on photodiode responsivity and signal amplification characteristics, I_0 is the power of the incident light beam, and σ is the parameter defining the width of the Gaussian beam at the detector. Eq. (2) can be transformed into a simpler form, using the variable substitution $\xi = (x - S)/\left(\sqrt{2}\sigma\right)$ and calculating the remainder of the integral difference in the above equation:

$$V = GI_0 erf\left(\frac{S}{\sqrt{2}\sigma}\right) \tag{3}$$

Using the equations above, we obtain:

$$V(\Delta P) = GI_0 erf\left(\frac{D}{\sqrt{2}\sigma}\frac{L\alpha\Delta P}{\Delta H}\right) \tag{4}$$

Note, that Eq. (4) shows that for an expanding beam the increase in the beam displacement value S with D will be compensated by the increase in Gaussian width. It follows that magnifying the deflection S with additional optical elements will not result in additional sensitivity gain.

The sensitivity of the PBDT is a function of several parameters that must be optimized to achieve maximum performance, and can be classified into the following two categories: (1) parameters dependent on, or related to, the probe beam, and (2) parameters dependent on the sensing element. In the first category are parameters such as the piezo-optic coefficient of the medium, the probe beam power, beam wavelength, beam diameter, beam collimation, interaction length, geometry of the pressure wave (spherical or planar), and the speed of sound and ambient temperature. In the second category are parameters such as the photodiode detector specifications (e.g. type, size, sensitivity and saturation), amplifier performance, and electronic circuit characteristics. Sensitivity improvement is ongoing and, if some of the parameters are optimized correctly, then sensitivity may be improved as much as two fold. Another issue that is being addressed is susceptibility to high electromagnetic interference, which has been observed in this open design and affects the performance of the pre-amplifier and the differential amplifier; better shielding and circuit layout will reduce this problem. Sensitivity is a function of probe beam intensity, but this parameter is limited due to saturation of the photodiode circuit; thus optimization of these parameters by careful selection of detector

components is critical to achieving maximum light intensity with a high saturation point.

3.5. Considerations for improvement of system scan time

The scan duration in this prototype system was primarily determined by the speed of the data acquisition system which required approximately 0.9 s/pixel. Thus, the 17,956 pixels in the $93.8 \times 93.8\ \mu m^2$ image required about 16,160 s, or just under 5 h, to acquire all the image data. Speeding up image acquisition, therefore, will primarily depend on designing a faster data acquisition system. A laser with a higher pulse repetition frequency will also contribute to faster image acquisition. The unit used in this prototype system had a maximum PRF of 20 Hz; in future versions a 1 KHz PRF tunable laser will be used. The higher PRF laser will also be useful if a greater number of averages, e.g. 64 or higher, is used to improve image quality. In the prototype system, image noise was introduced by several factors, including mechanical vibrations and drift of the mechanical components during the long scan time, as well as some instability of the excitation laser (the pulse to pulse variability in energy output contributed to image noise). In this case, signal averaging was useful for obtaining a good quality image. It is important to note that the PBDT sensor does not impose a limitation on the speed of image acquisition, which is determined by system parameters, e.g., data acquisition speed, laser PRF, and the time required to reposition the laser beam and/or the microscope stage.

4. Conclusions

As compared to piezoelectric methods of detection, PBDT offers a number or advantages due to its limited size and space requirements. Because the sensing beam is an extremely compact and non-interfering object, PBDT sensing can be easily integrated with any imaging method or technique that is used in an optical microscope, facilitating construction of multimodal imaging instruments. Due to the small probe beam diameter of less than 100 μm, PBDT can be used with the best high NA objectives to achieve maximum theoretical resolution. The beam can be positioned in close proximity to the origin of the ultrasound signals, where the pressure amplitude is the highest, resulting in additional gain of sensitivity. Finally, PBDT can be easily multiplexed, where multiple, non-interfering beams will be used to speed up the rate of image acquisition over a large area. Another major benefit of PBDT-based OAM is its simplicity to set up and adapt to virtually all types of objective lenses and samples, where the only requirement is to have a transparent sample holder or transparent coupling medium, both of which should be easily achieved.

The overall system performance depends on multiple, interacting factors. To improve the lateral and axial resolution in order to match the diffraction limit, deficiencies have to be eliminated in beam delivery, which fortunately is not affected by the optical sensing method. Improvements, such as better collimation of light at the objective lens, thereby achieving the complete filling of the objective aperture and perfect alignment of the excitation beam and the lens' optical axes, are needed to further enhance lateral and axial resolution.

A novel, non-contact, all-optical optoacoustic microscope is described in this work that utilizes the probe beam deflection technique (PBDT) to overcome a number of limitations in current implementations of OA microscopy. The suitability of this detection system for OA microscopy has been demonstrated. This design achieves lateral resolution of 0.5 μm and pressure sensitivity of better than 12 Pa in reflection mode. These parameters exceed most of those previously reported for OAM using piezoelectric and other non-optical detectors. The performance of this system warrants further development directed at improving the system resolution to match the theoretical diffraction limit and to improve the detector sensitivity. The all-optical passive sensing method promises to support more efficient OAM implementations with multiple imaging modalities than can be realized with conventional piezoelectric ultrasound hydrophones. Moreover, the system described here could easily be adapted to support *in vivo* microscopic imaging or even tomography. Future multi-modal OA imaging systems will enable new applications to perform multispectral analysis of the interactions of diverse targets such as cells and nanoparticles within live tissues.

Author contributions

S.M.M., D.A.T., C.C.R, A.A.O and R.D.G wrote the manuscript. S.M. M drew the images in Figs. 1(A and B), 2(A, and B). S.M.M and C.C.R conducted the experiments and analyzed the data. S.M.M., D.A.T, R. D.G., and A.A.O. proposed the concept of adapting the probe beam deflection technique to a microscopy platform suited for biological imaging. H.T.B, B.L.I, and S.M.M., were responsible for the experimental design. B.L.I and C.C.R received the funding that funded this project. H.T.B and B.L.I provided laboratory space and equipment necessary for this research. S.M.M, and B.L.I supervised the project. All authors discussed and contributed to the manuscript.

Conflict of interest

Drs. SM Maswadi and RD Glickman have an equity interest in EchoLase, Inc. Dr. AA Oraevsky has an equity interest in TomoWave Laboratories.

Acknowledgements

This work was supported by USAF AFMC 711th HPW/CL 2014 Chief Scientist Seedling Award (B. L. I.). Mr. Roth is a SMART Scholar and is supported by the OSD-T&E (Office of Secretary Defense-Test and Evaluation), Defense—Wide/PE0601120D8Z National Defense Education Program (NDEP)/BA-1, Basic Research. This study was also supported by a grant from the Air Force Office of Scientific Research (AFOSR-LRIR 139RH08COR). All work was performed at the Tri-Services Research Laboratories at Ft. Sam Houston, Texas. We thank Dr. Jingyong Ye, of the Department of Biomedical Engineering at the University of Texas at San Antonio, for a critical reading of the manuscript. This research was supported in part by NIH grant R43EB015287 (SMM, DAT, AAO).

References

[1] S. Hu, L.V. Wang, Neurovascular photoacoustic tomography, Front. Neuroenerg. 2 (2010) 10.
[2] S. Hu, L.V. Wang, Photoacoustic imaging and characterization of the microvasculature, J. Biomed. Opt. 15 (2010) 011101.
[3] C. Kim, C. Favazza, L.V. Wang, In vivo photoacoustic tomography of chemicals: high-resolution functional and molecular optical imaging at new depths, Chem. Rev. 110 (2010) 2756–2782.
[4] C. Li, L.V. Wang, Photoacoustic tomography and sensing in biomedicine, Phys. Med. Biol. 54 (2009) R59–R97.
[5] S. Mallidi, G.P. Luke, S. Emelianov, Photoacoustic imaging in cancer detection, diagnosis, and treatment guidance, Trends Biotechnol. 29 (2011) 213–221.
[6] L.V. Wang, Multiscale photoacoustic microscopy and computed tomography, Nat. Photonics 3 (2009) 503–509.

[7] K. Maslov, H.F. Zhang, S. Hu, L.V. Wang, Optical-resolution photoacoustic microscopy for in vivo imaging of single capillaries, Opt. Lett. 33 (2008) 929–931.
[8] C. Zhang, K. Maslov, L.V. Wang, Subwavelength-resolution label-free photoacoustic microscopy of optical absorption in vivo, Opt. Lett. 35 (2010) 3195–3197.
[9] S. Hu, K. Maslov, L.V. Wang, Second-generation optical-resolution photoacoustic microscopy with improved sensitivity and speed, Opt. Lett. 36 (2011) 1134–1136.
[10] H. Wang, X. Yang, Y. Liu, B. Jiang, Q. Luo, Reflection-mode optical-resolution photoacoustic microscopy based on a reflective objective, Opt. Express 21 (2013) 24210–24218.
[11] C. Zhang, K. Maslov, S. Hu, R. Chen, Q. Zhou, K.K. Shung, L.V. Wang, Reflection-mode submicron-resolution in vivo photoacoustic microscopy, J. Biomed. Opt. 17 (2012) 020501.
[12] H.F. Zhang, K. Maslov, G. Stoica, L.V. Wang, Imaging acute thermal burns by photoacoustic microscopy, J. Biomed. Opt. 11 (2006) 054033.
[13] G. Paltauf, R. Nuster, M. Haltmeier, P. Burgholzer, Photoacoustic tomography using a Mach–Zehnder interferometer as an acoustic line detector, Appl. Opt. 46 (2007) 3352–3358.
[14] T. Berer, H. Grün, C. Hofer, P. Burgholzer, Photoacoustic microscopy with large integrating optical annular detectors, Proc. SPIE 7371 (2009) 73710X (Novel Optical Instrumentation for Biomedical Applications IV).
[15] Z. Xie, S.L. Chen, T. Ling, L.J. Guo, P.L. Carson, X. Wang, Pure optical photoacoustic microscopy, Opt. Express 19 (2011) 9027–9034.
[16] A. Hochreiner, J. Bauer-Marschallinger, P. Burgholzer, B. Jakoby, T. Berer, Non-contact photoacoustic imaging using a fiber based interferometer with optical amplification, Biomed. Opt. Express 4 (2013) 2322–2331.
[17] E. Khachatryan, S. Maswadi, D.A. Tsyboulski, E. Barnes, D. Sardar, A.A. Oraevsky, K. Nash, R. Glickman, Optoacoustic microscopy using laser beam deflection technique, Proc. SPIE 8943 (2014) 89432T (Photons Plus Ultrasound: Imaging and Sensing).
[18] H. Li, B. Dong, Z. Zhang, H.F. Zhang, C. Sun, A transparent broadband ultrasonic detector based on an optical micro-ring resonator for photoacoustic microscopy, Sci. Rep. 4 (2014) 4496.
[19] L.V. Wang, S. Hu, Photoacoustic tomography: in vivo imaging from organelles to organs, Science 335 (2012) 1458–1462.
[20] W. Song, W. Zheng, R. Liu, R. Lin, H. Huang, X. Gong, S. Yang, R. Zhang, L. Song, Reflection-mode in vivo photoacoustic microscopy with subwavelength lateral resolution, Biomed. Opt. Express 5 (2014) 4235–4241.
[21] D.K. Yao, K. Maslov, K.K. Shung, Q. Zhou, L.V. Wang, In vivo label-free photoacoustic microscopy of cell nuclei by excitation of DNA and RNA, Opt. Lett. 35 (2010) 4139–4141.
[22] E.Z. Zhang, P.C. Beard, A miniature all-optical photoacoustic imaging probe, Proc. SPIE 7899 (2011) 78991F (Photons Plus Ultrasound: Imaging and Sensing).
[23] E. Zhang, J. Laufer, P. Beard, Backward-mode multiwavelength photoacoustic scanner using a planar Fabry–Perot polymer film ultrasound sensor for high-resolution three-dimensional imaging of biological tissues, Appl. Opt. 47 (2008) 561–577.
[24] S.M. Maswadi, R.D. Glickman, N. Barsalou, R.W. Elliott, Investigation of photoacoustic spectroscopy for biomolecular detection, Proc. SPIE 6138 (2006) 61380V (Ophthalmic Technologies XVI).
[25] S. Maswadi, L. Page, L. Woodward, R.D. Glickman, N. Barsalou, Optoacoustic sensing of ocular bacterial antigen using targeted gold nanorods, Proc. SPIE 6856 (2008) 685615 (Photons Plus Ultrasound: Imaging and Sensing).
[26] L. Page, S. Maswadi, R.D. Glickman, N. Barsalou, R. Branstetter, S. Thompson, Optoacoustic imaging: application to the detection of foreign bodies, Proc. SPIE 7177 (2009) 71770X (Photons Plus Ultrasound: Imaging and Sensing).
[27] R.A. Barnes Jr., S. Maswadi, R. Glickman, M. Shadaram, Probe beam deflection technique as acoustic emission directionality sensor with photoacoustic emission source, Appl. Opt. 53 (2014) 511–519.
[28] S.-L. Chen, L.J. Guo, X. Wang, All-optical photoacoustic microscopy, Photoacoustics 3 (2015) 143–150.
[29] K. Vedam, P. Limsuwan, Piezo-optic behavior of water and carbon tetrachloride under high pressure, Phys. Rev. Lett. 35 (1975) 1014–1016.
[30] J.M. Boone, J.A. Seibert, An analytical edge spread function model for computer fitting and subsequent calculation of the LSF and MTF, Med. Phys. 21 (1994) 1541–1545.
[31] E.J. Botcherby, C.W. Smith, M.M. Kohl, D. Debarre, M.J. Booth, R. Juskaitis, O. Paulsen, T. Wilson, Aberration-free three-dimensional multiphoton imaging of neuronal activity at kHz rates, Proc. Natl. Acad. Sci. U. S. A. 109 (2012) 2919–2924.
[32] A.M. Winkler, K. Maslov, L.V. Wang, Noise-equivalent sensitivity of photoacoustics, J. Biomed. Opt. 18 (2013) 097003.
[33] J. Yao, L.V. Wang, Sensitivity of photoacoustic microscopy, Photoacoustics 2 (2014) 87–101.

Dr. Saher M. Maswadi received a Ph.D. in applied physics from Hull University, United Kingdom in 2002. He then moved to University of Texas Health Science Center at San Antonio, Texas to work in research projects in the field of biomedical optics, laser ophthalmic, nanotechnology, biosensors, photoacoustics, and acoustic sensing technologies. Currently, Dr. Maswadi works in few projects at Ft. Sam Houston at the Air Force Research Laboratory and hold adjunct faculty positions at the University of Texas at San Antonio in the physics and electrical engineering departments. He is also a founder of EchoLase Inc working to develop laser-ultrasound systems.

Dr. Bennett L. Ibey is a Senior Research Biomedical Engineer with the 711th Human Performance Wing of the Air Force Research Laboratory, Radio Frequency Bioeffects Branch. He received a PhD in Biomedical Engineering from Texas A&M University in 2006 with a focus on biomedical optics. Since that time, his research interests have focused on the interaction between tissue and nanosecond pulsed electric fields and high peak power microwave bioeffects.

Mr. Caleb C. Roth, born in Bowie, Texas, received a B.A. degree in biology from Austin College in 2000 and a M.S. degree in biology from the University of Texas San Antonio in 2003. He is currently pursuing a Ph.D. degree in Radiation Biophysics from University of Texas Health Science Center San Antonio. Mr. Roth is a SMART Scholar (The Science, Mathematics and Research for Transformation Scholarship for Service Program) cohort 2012. Mr. Roth studies the biological effects of nanosecond electrical pulse generated shock waves on cells grown in culture. He conducts research at Ft. Sam Houston in San Antonio, Texas at the Air Force Research Laboratory (AFRL/RHDR).

Dr. Dmitri A. Tsyboulski worked as a Senior Scientist at TomoWave Laboratories, Inc. (Houston, TX). He obtained his Ph.D. in Chemistry from Rice University, Houston, TX in 2006. His research expertise includes design of spectroscopic and imaging systems, nanoparticle characterization, and molecular spectroscopy. Currently Dmitri is working as a Senior Research Engineer at the Allen Institute for Brain Science.

Dr. Hope Beier has been a Research Biomedical Engineer in AFRL's Optical Radiation Bioeffects Branch since November 2012. She serves as a principal investigator for efforts using advanced optical techniques to investigate the effects of directed energy (laser and radio frequency) on biology. Dr. Beier received her Ph.D. in Biomedical Engineering in 2009 from Texas A&M University. She joined AFRL in 2010 as a National Research Council Postdoctoral Research Associate.

Dr. Randolph D. Glickman holds the Senderoff Professorship of Vision Research in the Department of Ophthalmology at the University of Texas Health Science Center at San Antonio. Author of 115 journal articles, dozens of technical reports and conference proceedings, and an editor (along with K. Hardy and M. Meltz) of the textbook, "Non-Ionizing Radiation Biology: An Overview of the Physics and Biology", Dr. Glickman is recognized as an authority on laser-tissue interaction, applications of biomedical optics, and nanobiotechnology. Dr. Glickman is currently the President of the Alamo Chapter of Sigma Xi, from which he received the Martin Goland Research Award in 2007. In 2015, along with several colleagues, he founded EchoLase, Inc., to commercialize all-optical detector technology for use in ultrasound imaging.

Dr. Alexander A. Oraevsky has 25 years of experience managing research and development laboratories in academia and small businesses. He is a pioneer in the field of biomedical optoacoustics. Presently he leads TomoWave Laboratories as Chief Technology Officer and holds an adjunct Professor position at the Biomedical Engineering Department of the University of Houston. Dr. Oraevsky is the recipient of multiple research awards advancing biomedical applications of the optoacoustic imaging sensing and monitoring, including Berthold Leibinger Innovations Prize. Alexander is the primary inventor of 20 patents, has published seven book chapters and over 200 scientific papers dealing with novel laser technologies applicable in biology and medicine.